Inorganic Chemistry

Article

Cite This: Inorg. Chem. XXXX, XXX, XXX−XXX

pubs.acs.org/IC

Reversible and Sensitive Hg^{2+} Detection by a Cell-Permeable Ytterbium Complex

Guochen Bao,[†,‡] Shuai Zha,[†] Zhenyu Liu,[§,∥] Yan-Ho Fung,[†] Chi-Fai Chan,[†] Hongguang Li,[†] Pak-Ho Chu,[†] Dayong Jin,*[,‡] Peter A. Tanner,*[,†] and Ka-Leung Wong*[,†]

[†]Department of Chemistry, Hong Kong Baptist University, Kowloon Tong, Hong Kong SAR, People's Republic of China

[‡]Institute for Biomedical Materials and Devices (IBMD), Faculty of Science, University of Technology Sydney, Sydney, New South Wales 2007, Australia

[§]Department of Applied Biological and Chemical Technology, The Hong Kong Polytechnic University, Hung Hom, Hong Kong SAR, People's Republic of China

[∥]Department of Applied Biological and Chemical Technology, The Hong Kong Polytechnic University Shenzhen Research Institute, Shenzhen 518057, People's Republic ofChina

Supporting Information

ABSTRACT: A cell-permeable ytterbium complex shows reversible binding with Hg^{2+} in aqueous solution and in vitroby off−on visible and NIR emission. The fast response and 150 nM sensitivity of Hg^{2+} detection is based upon FRET and the lanthanide antenna effect. The reversible Hg^{2+} detection can be performed in vitro, and the binding mechanism is suggested by NMR employing the motif structure in a La complex and by DFT calculations.

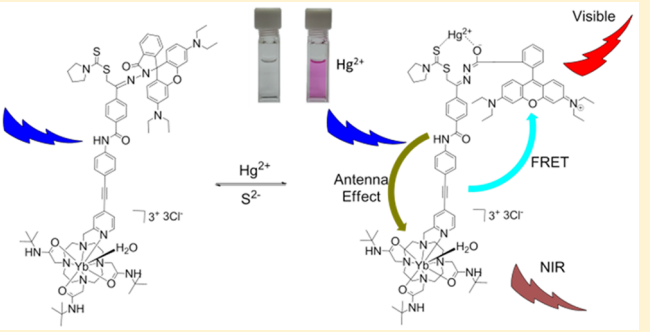

INTRODUCTION

Heavy metal pollution has exceeded regulatory limits in many parts of the world due to the rapid and careless development of industries, and this problem has increasingly gained concern.[1] Among the hazardous contaminants, the mercury(II) ion is notably one of the most dangerous threats to human health due to its strong affinity toward thiol groups, resulting in the dysfunction of most proteins and enzymes.[2] Moreover, with its persistent bioaggregation and nonbiodegradability, this pollutant can accumulate in the human body through the food chain; even at low concentrations it causes harmful diseases such as brain and nervous system damage, kidney failure, and cognitive disorder.[3−7] Therefore, concerns over the wide-reaching hazards of mercury have motivated chemists to develop selective Hg^{2+} probes for biological and environmental sensing and monitoring applications.

Fluorescent sensors enable quantitative detection of heavy metal ion concentrations and are useful tools for monitoring mercury contamination. Considerable efforts have been made to develop various fluorescence-based sensors such as with the use of rosamine,[8] semisquaraines,[3] and porphyrins.[9] The rhodamine B based sensor is a reversible chemosensor with a novel design.[10] The metal-induced ring-opening process offers distinct photophysical advantages in terms of sensitivity, selectivity, and response time.[4,11] However, just as for other organic dye based sensors, significant challenges still need to be overcome. Most sensors require a mixed solution of water and organic solvent due to their poor water solubility.[6,9−11] The narrow Stokes shift of the organic dye also limits its applications due to the interference of exciting light.[6,11] Fluorescence resonance energy transfer (FRET) is a tool to overcome this problem for the chemical sensing of ions.[12] FRET is based upon the strong distance-dependent interaction between an excited donor and an acceptor, permitting clear observation of the acceptor emission.[13] Lanthanide chelates are good candidates for the development of luminescence sensors, possessing wide wavelength shifts between the donor absorption and metal acceptor emission, long luminescence lifetimes (microsecond to millisecond), and characteristic, sharp luminescence.[14−18] Our previously reported Yb(III)-based Hg^{2+} sensor **YbPor-L** exhibited some of these characteristics with reasonable sensitivity and selectivity.[9] Notably, the sensor emission is located in the NIR spectral region and can penetrate biological tissues. However, the sensor suffers from poor water solubility, only having response in mainly organic solvents, and it cannot be incorporated into living cells or tissues. The detection limit is insensitive for many applications, lying on the micromolar scale (10 μM) in a mixed solution of organic solvent and buffer.[9] Furthermore, the wavelength of the

Received: August 31, 2017

DOI: 10.1021/acs.inorgchem.7b02243
Inorg. Chem. XXXX, XXX, XXX−XXX

visible response signal is very close to the excitation wavelength. These drawbacks make it unsuitable for use in cells and spurred us to develop a more sensitive and biocompatible probe for Hg^{2+} monitoring.

Herein, we report the design and synthesis of a dual channel sensor, **GBYb001**, the combination of an Yb^{3+}-based complex with a rhodamine B sensing unit (Figure 1). By introduction of

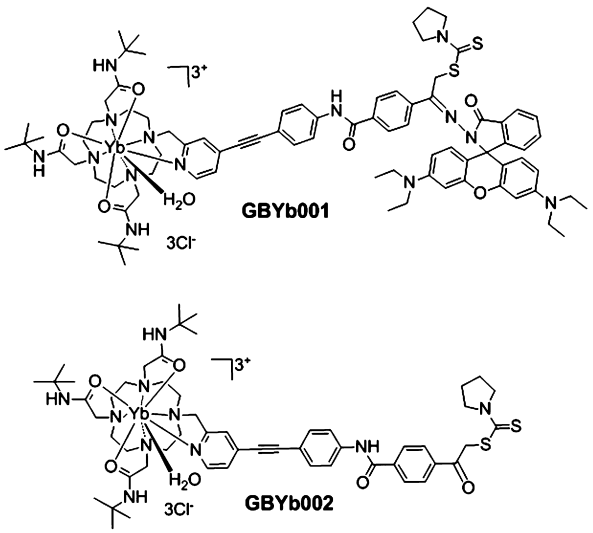

Figure 1. Structure of complexes **GBYb001** and **GBYb002**.

an amide chain substituted cyclen as the coordinating unit of the Yb^{3+} cation, the resulting positively charged complex exhibited excellent water solubility. A carbodithioate moiety serves as the "catching" unit of Hg^{2+}. Moreover, it then triggers the ring-opening process of the rhodamine B unit, which gives the sensor high selectivity and sensitivity. The construction is completed with the well-designed substituted 4-(phenylethynyl)pyridine (**py**) unit, which harvests photons and transfers energy through FRET to the ring-opened rhodamine B and Yb^{3+} ions. This new sensor displays selective turn-on emission responses in both the visible and NIR regions in the presence of Hg^{2+}. Both emission channels are far removed from the excitation wavelength, and the quick detection response, low detection limit, and reversible property make it practical for biological applications.

RESULTS AND DISCUSSION

GBYb001 was synthesized by connecting a three-chain-substituted cyclen with the **py** moiety and carbodithioic and rhodamine B fragments through a series of synthetic steps and then coordinating with Yb^{3+} in aqueous MeOH (Scheme 1). Compounds **3**, **5**, and **7** were synthesized according to the literature[9,19,20] (Schemes S1–S3 in the Supporting Information). Compound **10** was synthesized by Sonogashira coupling of compound **7** with *tert*-butyl (4-iodophenyl)carbamate to form compound **8**, followed by substitution with compound **5** and N-Boc deprotection.[19] Compound **11** was synthesized via amidation of intermediate **10** with compound **3** at room temperature. Compound **11** was then substituted with hydrazine hydrate and rhodamine B to form ligand **13** (**GB001**),[9] which was followed by coordination with Yb^{3+} to form the complex **GBYb001**. The control **GBYb002** was also synthesized together with the intermediate **11** (**GB002**) using the same strategy (Schemes 1 and Scheme S4 in the Supporting Information). All of the target products and intermediates were fully characterized by various spectroscopic techniques, as detailed in the Supporting Information.

In HEPES buffer, **GBYb001** exhibits the intense absorption of the **py** moiety, with a maximum at 325 nm (ε = 26180 M^{-1} cm^{-1}), together with the characteristic absorption of rhodamine B indicated by the weak band at 565 nm (Figure S4 in the Supporting Information). Upon photoexcitation of the **py** chromophore, the complex displayed a weak red emission (λ_{max} 591 nm), corresponding to the $\pi \rightarrow \pi^*$ transition of the rhodamine B moiety. The emission of the substituted pyridine unit was almost quenched due to FRET (Figure S5 in the Supporting Information). This is demonstrated in the excitation spectrum of rhodamine B emission (Figure S6 in the Supporting Information), where not only rhodamine B absorption but also the substituted pyridine absorption is present. Hence, the rhodamine B emission can be well-separated from the excitation wavelength. There is an efficient spectral overlap between the emission spectrum of the intermediate **11** (**GB002**, part of **GBYb001**) and the excitation spectrum of the rhodamine B unit (Figure S7 in the Supporting Information). The room-temperature emission of **11** is deemed to originate from a singlet excited state, and it is quenched in the presence of the lanthanide ion in **GBYb001**.

Under 355 nm excitation of **GBYb001** in CH_3CN solvent, a weak characteristic NIR emission (around 980 nm) is also observed, due to the intraconfigurational $^2F_{5/2} \rightarrow {}^2F_{7/2}$ transition of Yb^{3+} (Figure S8 in the Supporting Information). Since Yb^{3+} does not have an absorption band at the excitation wavelength, the emission is due to energy transfer to the Yb^{3+} acceptor from the **py** chromophore or rhodamine B donor. Direct excitation at 570 nm does not excite Yb^{3+} emission so that the donor to the Yb^{3+} acceptor is the **py** chromophore. The donor nonradiative transition is electric dipole allowed, and that of the acceptor is electric quadrupole and forced electric dipole allowed.

Upon addition of Hg^{2+} ion (using $Hg(ClO_4)_2$ as the source; note that metal perchlorates are usually explosive and should be used with caution[21]) to the buffered solution of **GBYb001**, the solution turned from colorless to red within 1 s. Consequently, a 22-fold enhancement of absorption intensity was observed (with a 10 nm bathochromic shift) for the 575 nm peak (Figure 2). At the same time, the absorption band at 325 nm decreased slightly in intensity. This is not due to dilution but indicates a structural change of the complex. However, no obvious change was observed for a similar addition of Hg^{2+} to a solution of the control compound **GBYb002** (Figure S10 in the Supporting Information). This demonstrates that **GBYb001** exists in the spirocyclic form and that the addition of Hg^{2+} triggers ring opening to occur. It takes place rapidly in the buffer solution at room temperature. The binding stoichiometry of **GBYb001** was determined to be 1:1 by a Job plot from the absorption spectrum, where the absorbance at 575 nm reaches a maximum when the mole fraction is 50% (Figure 2, inset). The binding constant for Hg^{2+} in buffer solution with **GBYb001** was evaluated by nonlinear least-squares analysis[22] of the absorption intensity at 575 nm: $K_b = (2.05 \pm 0.30) \times 10^5$ M^{-1}.

The changes in fluorescence intensity of **GBYb001** were measured in HEPES buffer solution or in CH_3CN. Upon the addition of Hg^{2+}, **GBYb001** exhibited a significant turn-on emission in both the visible (~596 nm) and NIR regions (~980 nm) upon excitation of the **py** unit (Figure 3). We rationalize that the visible emission enhancement at 596 nm

DOI: 10.1021/acs.inorgchem.7b02243
Inorg. Chem. XXXX, XXX, XXX–XXX

Scheme 1. Synthesis of Hg^{2+} Probe GBYb001 and its La Structure Motif Complex GBLa001[a]

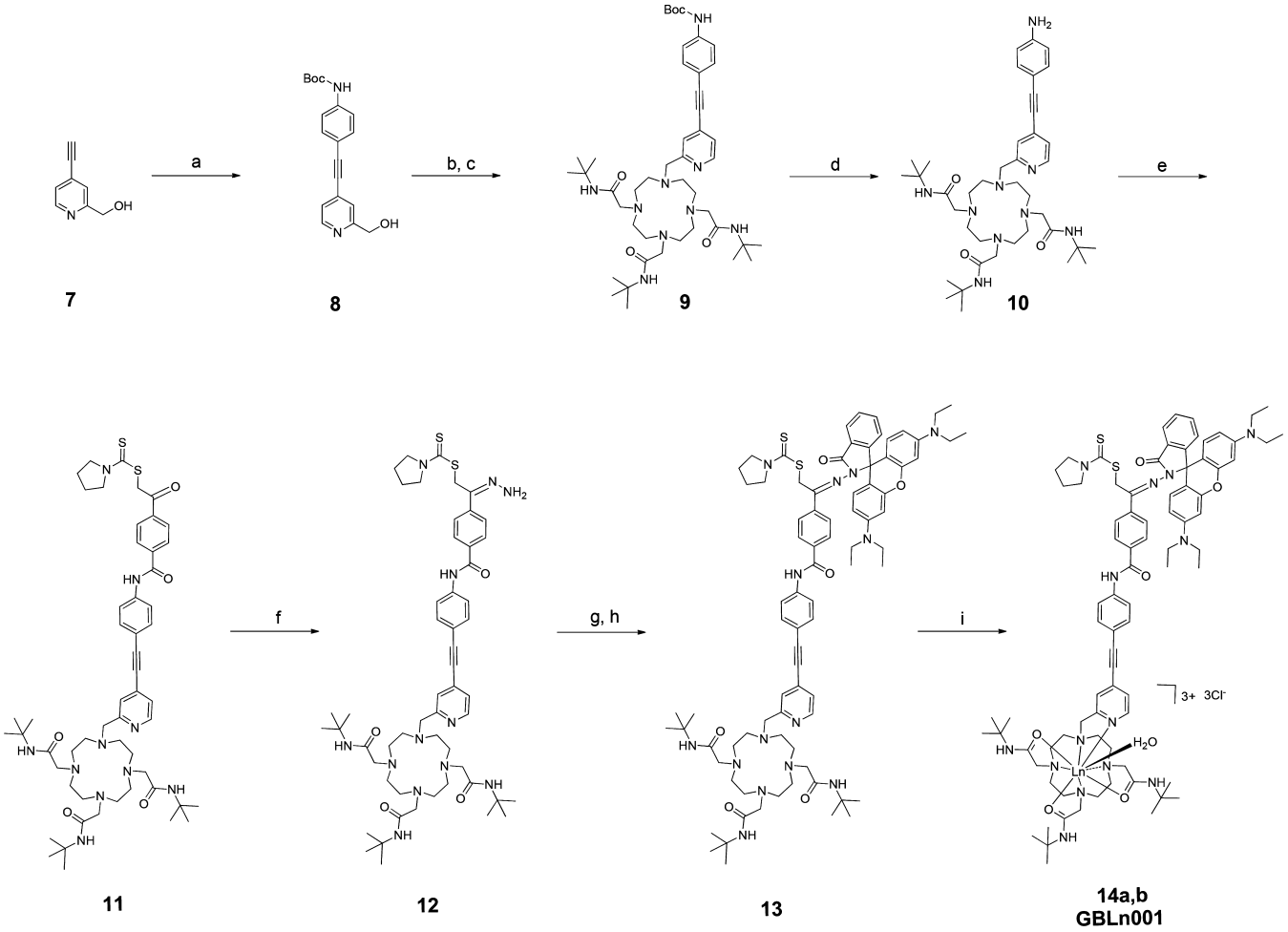

[a]Legend: (a) $Pd(PPh_3)_4$, CuI, *tert*-butyl (4-iodophenyl)carbamate, DIPEA, THF, room temperature, 3 days; (b) MsCl, DIPEA, DCM, room temperature, 1 h; (c) K_2CO_3, **5**, CH_3CN, 50 °C, 19 h; (d) HCl(aq), MeOH, 0 °C to room temperature, 6 h; (e) **3**, EDCI, HOBt, DIPEA, CH_3CN, room temperature, 36 h; (f) hydrazine hydrate, acetic acid, THF, EtOH, reflux, 2 h; (g) rhodamine B, $POCl_3$, Et_3N, 1,2-dichloroethane, reflux, 5 h; (h) Et_3N, DCM, room temperature, 12 h; (i) $LnCl_3$(aq), MeOH, room temperature, 24 h.

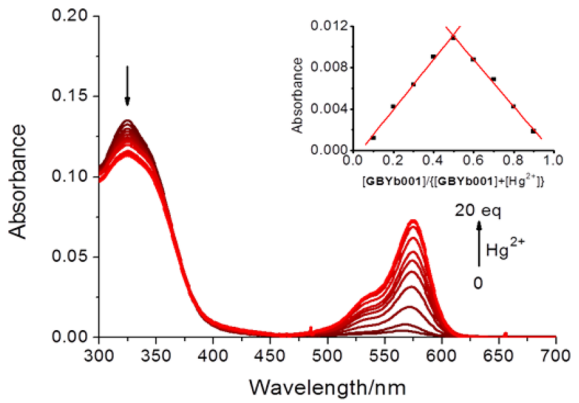

Figure 2. Changes in the absorption spectrum of **GBYb001** (5 μM) in HEPES buffer solution upon titration with Hg^{2+} (0 → 20 equiv). Inset: Job plot at 575 nm of this addition, [**GBYb001**] + [Hg^{2+}] = 5 μM.

occurs because of the increase in absorption of the rhodamine B moiety (hence the increased spectral overlap) induced by the ring-opening mechanism, thereby enabling more efficient FRET from the **py** chromophore to the rhodamine B fragment. The excitation spectra following the addition of Hg^{2+} to **GBYb001** exhibit an enhancement of rhodamine B fluorescence when either the **py** moiety or the rhodamine B unit is excited (Figure S6 in the Supporting Information). The normalized excitation spectra, before and after addition of Hg^{2+} (Figure S11 in the Supporting Information), show that the relative increase of intensity of the **py** moiety excitation band is greater than that of the rhodamine B excitation band. Hence, the energy transfer from **py** is more efficient for the ring-opened form. Figure 3 shows that the observed enhancement of emission intensity is linearly proportional to the concentration of Hg^{2+} up to the saturation limit (~20 μM), and the limit of detection (LOD) is estimated to be 150 nM (Figure S12 in the Supporting Information). This LOD is 67 times lower than that of our previously reported mercury sensor YbPor-**L**.[9] The enhancement of NIR emission from Yb(III) ($^2F_{5/2} \rightarrow {}^2F_{7/2}$) is due to the absorption band shift of the chromophore unit in CH_3CN (Figure S13 in the Supporting Information): the energy is transferred from the **py** chromophore to Yb(III) through the antenna effect so that there is a wide wavelength gap between excitation and emission. However, no Yb(III) emission is observed under 570 nm excitation, when the rhodamine unit is excited, indicating the absence of energy transfer from rhodamine B to

DOI: 10.1021/acs.inorgchem.7b02243
Inorg. Chem. XXXX, XXX, XXX−XXX

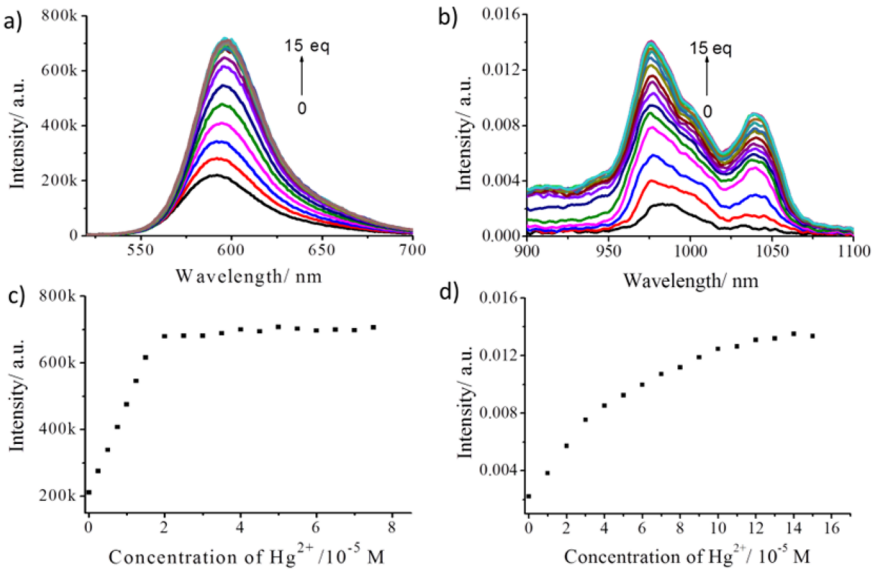

Figure 3. (a) Visible fluorescence response (λ_{ex} 346 nm) of **GBYb001** (5 μM) upon addition of Hg^{2+} in HEPES buffer. (b) NIR emission (λ_{ex} 355 nm) of **GBYb001** (10 μM) in CH_3CN upon addition of Hg^{2+}. (c, d) Plots of the enhancement at 596 and 980 nm, respectively.

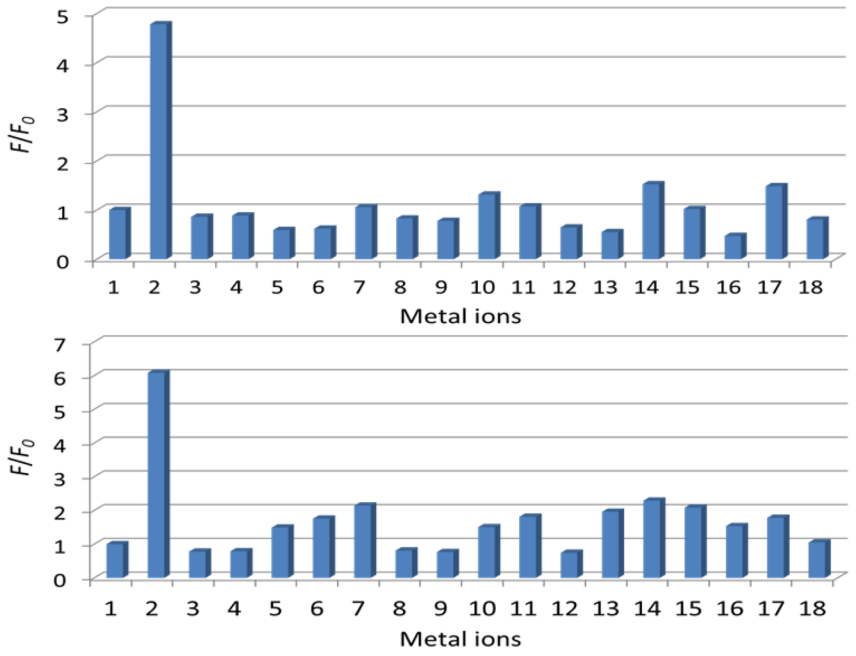

Figure 4. (a) Visible fluorescence ratio of **GBYb001** (5 μM, λ_{ex} 525 nm) in HEPES buffer at 596 nm and (b) NIR emission ratio of **GBYb001** (10 μM, λ_{ex} = 355 nm) in CH_3CN (with 1% of water) at 980 nm. Metal ions: 1, blank (normalized as F_0); 2, Hg^{2+}; 3, Cu^{2+}; 4, Cu^{+}; 5, Co^{2+}; 6, Cd^{2+}; 7, Ca^{2+}; 8, K^{+}; 9, Li^{+}; 10, Fe^{3+}; 11, Fe^{2+}; 12, Cs^{2+}; 13, Mg^{2+}; 14, Pb^{2+}; 15, Sn^{2+}; 16, Ni^{2+}; 17, Al^{3+}; 18, Na^{+}.

Yb^{3+}. The decay of NIR emission of **GBYb001** in CH_3CN after the addition of Hg^{2+} is monoexponential with a lifetime of 2.31 μs (Figure S14 in the Supporting Information) and with a quantum yield of 0.014% (Figure S15 in the Supporting Information). This long lifetime distinguishes the sensor from fluorescent organic dyes with nanoscale lifetimes, and the limit of detection is estimated to be 5.0 μM (Figure S16 in the Supporting Information), which is 2 times lower than that in our previous work.[9] Moreover, with emission lying in the first biological window, which has less light scattering, low skin absorption, and hence enhanced escape from deeper tissues,[23] the NIR emission makes our sensor potentially suitable for biological applications.

To verify the sensor specificity, both the visible and NIR dual-response emission spectra of **GBYb001** were examined in the presence of various environmentally and biologically important metal ions, under the same conditions as for Hg^{2+} ions. The presence of common ions in cells, Na^{+}, K^{+}, Ca^{2+}, and Mg^{2+}, caused little change in the visible or NIR emission and did not interfere with the binding of Hg^{2+}, even at 1 mM concentration (Figure 4 and Figure S17 in the Supporting Information). The **GBYb001** sensor was also selective for Hg^{2+} in comparison with a wide range of other heavy metal, transition metal, alkali metal, and alkali earth metal ions (Figure 4). Such discriminatory photophysical properties in both the

DOI: 10.1021/acs.inorgchem.7b02243
Inorg. Chem. XXXX, XXX, XXX−XXX

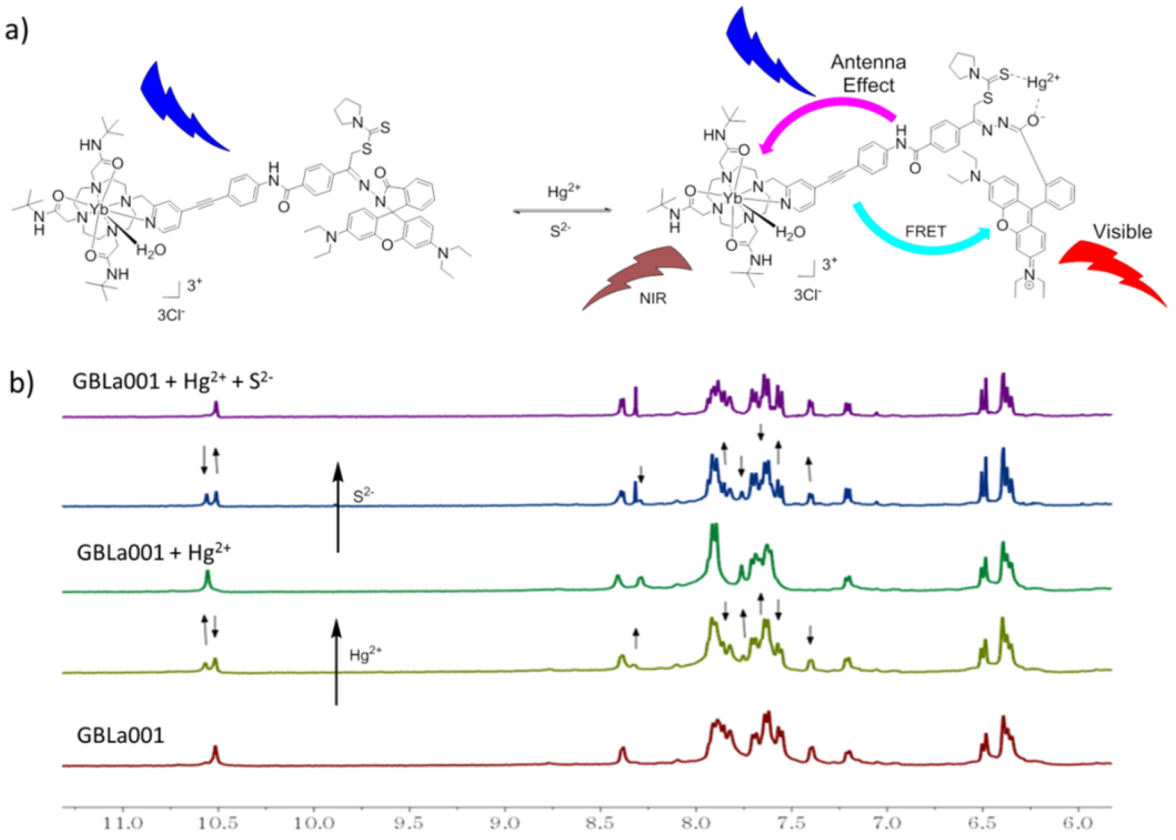

Figure 5. (a) Proposed mechanism of spiro-ring-opening and -closing process triggered by Hg^{2+} and S^{2-}. (b) ^1H NMR spectra of **GBLa001** in d_6-DMSO upon addition of Hg^{2+} and then S^{2-}.

visible and NIR ranges indicate the potential application for biological samples.

The reversibility of **GBYb001** upon Hg^{2+} binding was next investigated. Cellular thiol compounds, such as cysteine, glutathione (GSH), and various thiol-containing peptides and proteins, play crucial roles in mercury detoxification.[8] Because of the high binding ability of Hg^{2+} toward these cellular compounds, it is predicted that the thiol group will strip the bound Hg^{2+} from the **GBYb001-Hg** complex, resulting in the recovery of the low-fluorescent Hg^{2+}-free sensor. Taking advantage of its high dissociation ability in buffer solution, we chose Na_2S as the thiol source to examine the reversibility. As expected, upon addition of S^{2-} anions to the solution of **GBYb001-Hg**, an immediate decrease in fluorescence intensity to the initial level of the free probe was observed. The enhancement of emission could be recovered when Hg^{2+} was added again to the buffer solution (Figure S18 in the Supporting Information). The stability of **GBYb001** estimated by HPLC (Figures S19 and S20 in the Supporting Information) shows that **GBYb001** is relatively stable in HEPES buffer and even in the presence of S^{2-}. This reversible binding property of **GBYb001** and Hg^{2+} suggests that this probe could be used to monitor not only the cellular uptake of mercury ions but also the increase of the cellular thiol groups, which eliminates the cellular uptaken mercury in vivo.

In order to investigate the mechanism of spiro ring opening and recovery, ^1H NMR using a motif structure of the Yb complex, **GBLa001**, was performed to evaluate its interaction with Hg^{2+} and S^{2-} in DMSO-d_6 (Figure 5 and Figure S21 in the Supporting Information). The signal at 10.52 ppm, which is ascribed to the amide between the two aromatic rings, was slightly shifted downfield to 10.55 ppm upon addition of Hg^{2+} ions. The signal at 7.39 ppm disappeared, whereas a new signal at 8.28 ppm appeared. These features are assigned respectively to the aromatic hydrogens which are adjacent to the spiro carbon and the carbonyl group of the spiro ring. These hydrogens exhibited a large downfield shift due to the electron-withdrawing effect of Hg^{2+} connected to the oxygen anion generated by the ring-opening process. The other hydrogens on the same aromatic ring also showed slight downfield shifts. Similar shifts could also be found for hydrogens on the other two phenyl groups, while the hydrogens on the pyridine ring (8.38 and 7.20 ppm) and the tricyclic ring of the rhodamine unit (6.32−6.52 ppm) exhibited no change. The ^1H NMR spectrum also provides evidence for the reversibility of this probe. Upon addition of S^{2-}, the signals recovered their initial positions due to the removal of Hg^{2+} by the S^{2-} anion, while the oxygen anion was recovered to the amide group and the ring was closed. This correlated with the change in **GBYb001** emission upon binding with Hg^{2+} and S^{2-}.

The enhancement of the energy transfer mechanism for the ring-opened form was probed by DFT calculations[24−26] upon molecular fragments of **GBYb001** (refer to the Supporting Information). The relative geometry of the rhodamine and the **py** part is displayed in Figure 6a. The HOMO and LUMO of the **py** moiety are shown in Figure 6b, and the lowest singlet transition is mainly polarized along the triple bond axis. Figure 6c,d show the ring-closed and ring-opened fragments, respectively. The lowest singlet transition is more intense for the ring-opened form and the respective $S_0 \rightarrow S_1$ transitions are almost orthogonally polarized, with that of the ring-opened form more nearly parallel to the **py** axis. Importantly, the

DOI: 10.1021/acs.inorgchem.7b02243
Inorg. Chem. XXXX, XXX, XXX−XXX

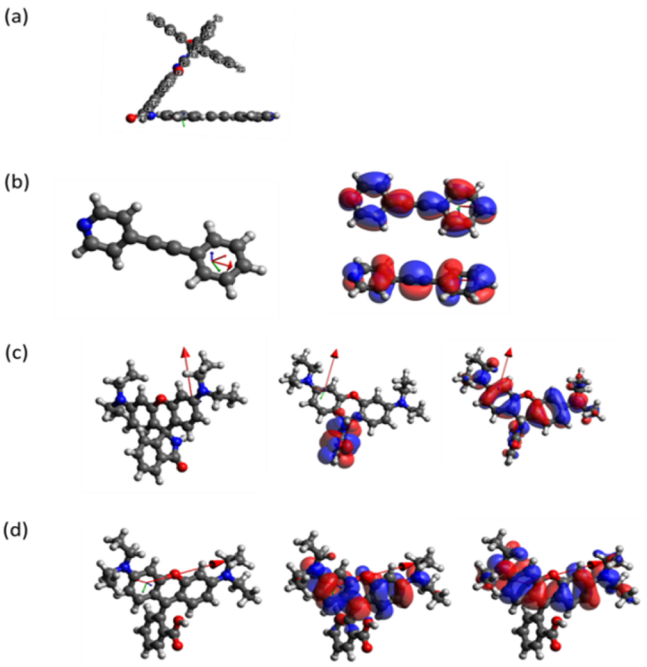

Figure 6. (a) Orientation of **py** and rhodamine parts. (b) **py** fragment with LUMO (top) and HOMO (bottom). (c) Ring-closed fragment with LUMO (left) and HOMO (right). (d) Ring-opened fragment with LUMO (left) and HOMO (right). The dipole moments are indicated by red arrows.

electron delocalization across three rings exists in the ring-opened form but is broken in the ring-closed form.

The practical application of **GBYb001** in fluorescence imaging for Hg^{2+} was investigated in living cells using confocal imaging microscopy. MRC-5 cells incubated with **GBYb001** (5 μM) exhibited very weak but detectable fluorescence in the living cells. However, a gradual increase in fluorescence was observed after the cells were incubated with 2.5, 5, and 10 μM of Hg^{2+} for 0.5 h at 37 °C in the dark (Figure 7a–d). In order to investigate the reversible fluorescence response of **GBYb001** in living cells, the same cells treated with 10 μM of Hg^{2+} were then exposed to 1 mM of S^{2-} for 1 h at 37 °C in the dark. The observed increase in fluorescence was reversed back to the original levels (Figure 7e). These results are consistent with the observation in HEPES buffer that S^{2-} reversibly recovered the Hg^{2+}-free sensor. Cellular uptake efficiency and cytotoxicity are vital properties for a real-time biosensor which can sensitively monitor biosamples. The MTT reduction assay of **GBYb001** on MRC-5 cells indicated low cytotoxicity after their treatment with various concentrations in the dark for 24 h, with an IC_{50} value of 88.5 μM (Figure S22 in the Supporting Information). The cellular uptake was investigated via flow cytometry by treating MRC-5 cells with the probe for different times. As shown in Figure S23 in the Supporting Information, **GBYb001** showed excellent cellular uptake in living MRC-5 cells and almost reached a maximum within 0.5 h. The cellular experiment results indicate that **GBYb001** is suitable for visualizing the change in intracellular concentration of Hg^{2+} and also could be used to monitor detoxification of biological thiol species toward Hg^{2+} at cellular levels.

CONCLUSIONS

In summary, the reversible dual-channel FRET and antenna effect based sensor **GBYb001** was designed and synthesized by combination of an ytterbium complex and a rhodamine B unit. The sensor exhibited high selectivity and sensitivity and quick response time to Hg^{2+} ions with responding visible and NIR signals. The ring-opening and recovery mechanism was deciphered by ^1H NMR spectra, employing the structure motif of the analogous La complex. With large excitation–emission wavelength shifts on both emission channels and excellent water solubility, **GBYb001** was successfully employed to monitor the changes of Hg^{2+} in living cells.

EXPERIMENTAL SECTION

Materials and Characterization. All chemicals were purchased and used as received without further purification. The solvents specified were dried by standard procedures. NMR spectra were recorded on a Bruker400 (400 Hz) nuclear magnetic resonance spectrometer with chemical shifts expressed as parts per million (ppm) and coupling constants J as hertz (Hz). High-resolution mass spectra

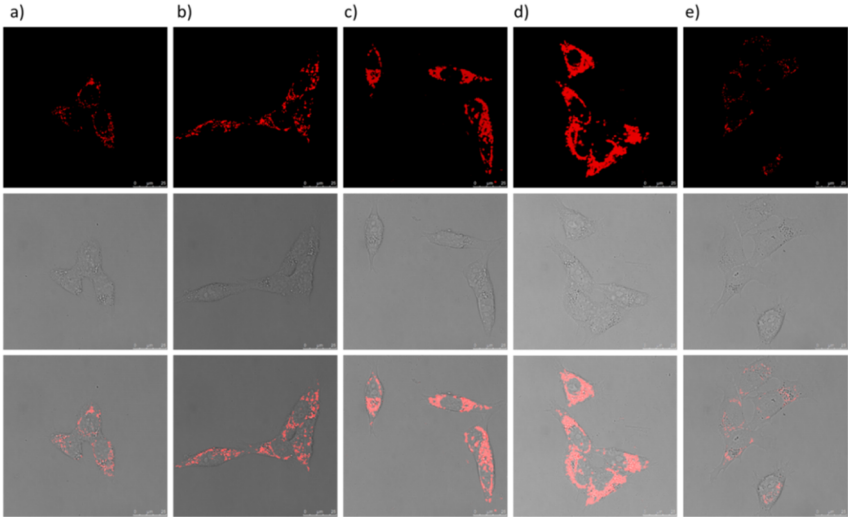

Figure 7. Confocal microscopic images of MRC-5 cells pretreated with 5 μM of **GBYb001** for 1 h and then treated with (a) 0 μM, (b) 2.5 μM, (c) 5 μM, and (d) 10 μM Hg^{2+} for 0.5 h. (e) Fluorescence images of the same cells of (d) further treated with 1 mM of S^{2-} and incubated for 1 h. The top row gives fluorescence images, the middle row bright field images, and the bottom row overlays.

DOI: 10.1021/acs.inorgchem.7b02243
Inorg. Chem. XXXX, XXX, XXX–XXX

were taken on a Bruker Autoflex matrix assisted laser desorption/ionization time-of-flight (MALDI-TOF) instrument or an electrospray ionization (ESI) mass spectrometer.

Photophysical Measurements. UV/vis spectra were recorded with an Agilent Cary 8454 UV−vis spectrophotometer. The measurements of emission and excitation spectra, emission decay, and quantum yield were performed using a Horiba Fluorolog-3 spectrofluorometer with a xenon lamp or a Nd^{3+}:YAG laser as excitation source. The visible range measurements were recorded using HEPES buffer (1 mM, pH 7.4), whereas those in the NIR spectral range were made with the use of CH_3CN. The metal ion sources (note that metal perchlorates are usually explosive and should be used with caution[21]) for the selectivity experiment were taken from $Hg(ClO_4)_2\cdot 6H_2O$, $CuCl_2$, $Co(ClO_4)_2\cdot 6H_2O$, $Cd(ClO_4)_2\cdot 6H_2O$, $CaCl_2$, KBr, LiBr, $Fe(NO_3)_3\cdot 9H_2O$, $FeCl_2\cdot 4H_2O$, Cs_2CO_3, $MgSO_4$, $Pb(NO_3)_2$, $SnCl_2\cdot 2H_2O$, $Ni(ClO_4)_2\cdot 6H_2O$, $Al(NO_3)_3\cdot 9H_2O$, NaCl, and $Cu(CH_3CN)_4PF_6$. These metal species are soluble in water (Table S2 in the Supporting Information). The aqueous solutions ($Cu(CH_3CN)_4PF_6$ used a solvent mixture of water and CH_3CN) of these metal salts were used to prepare the final metal cation solutions of 0.05 mM in HEPES buffer and 0.1 mM in CH_3CN (with 1% of water). The metal ion solutions in both water and CH_3CN (with 1% of water) were clear without any precipitate. To further confirm the dissolution of these salts in the solvent CH_3CN (with 1% of water), we dissolved each salt in CH_3CN/water (v/v = 99/1). The results showed that all these salts can be well dissolved at a concentration of 0.1 mM in this solvent. Quantum yields, Φ_Y, were measured using the standard $Yb(tta)_3phen$ (1.1% NIR emission quantum yield in toluene) according to the formula[27]

$$\Phi_Y = (G_Y/G_S)(n_Y/n_S)^2\Phi_S \quad (1)$$

where G is the slope of the plot of integrated emission intensity vs absorbance, n is the refractive index of the solvent employed, Φ is the quantum yield, Y represents the sample to be measured, and S is the standard sample.

Binding Constant. The binding constant K_b was obtained by a nonlinear least-squares analysis of the absorption or emission spectrum of the material versus concentration of Hg^{2+} with the formula:[22]

$$Y = Y_0 + \frac{Y_{lim} - Y_0}{2c_L}\left[\left(c_L + c_{Hg} + \frac{1}{K_b}\right) - \sqrt{\left(c_L + c_{Hg} + \frac{1}{K_b}\right)^2 - 4c_L c_{Hg}}\right] \quad (2)$$

where Y is the measured intensity (absorption or emission), Y_0 is the initial value (without addition of Hg^{2+}), Y_{lim} is the limiting value, and c_L and c_{Hg} are the concentrations of ligand and Hg^{2+}, respectively.

HPLC Analysis. The measurements of complexes using reverse-phase HPLC were conducted at room temperature using an Agilent 1200 HPLC system with DAD (column: Vision HT C18 HL 5 u, length 250 mm, Serial No. 5151920, i.d. 4.6 mm). The mobile phase was Milli-Q water (with 0.05% trifluoroacetic acid) and CH_3CN with a flow rate of 1 mL/min. The solvent gradient ratio is given in Table S1 in the Supporting Information.

Cell Culture. Human normal lung fibroblast (MRC-5) cells were maintained in minimum essential medium (MEM) supplemented with 10% fetal bovine serum (FBS) and antibiotics (penicillin, 50 mg mL^{-1}; streptomycin, 50 mg mL^{-1}). The cells were incubated at 37 °C in a humidified environment with 5% CO_2.

In Vitro Confocal Microscopy. To investigate the suitability of the mercury sensor for bioapplications, MRC-5 cells (1×10^5) were imaged. After incubation with 5 μM **GBYb001** for 1 h, x equiv (x = 0.5, 1, 2) of Hg^{2+} ions was loaded for further 0.5 h incubation. Then the cells were washed with PBS three times before imaging. After imaging, the cells (with 2 equiv of Hg^{2+}) were further incubated with 1 mM Na_2S for 1 h, and images were taken again to test the reversibility in living cells. All of the images were acquired on a Leica TCS SP8 confocal laser-scanning microscope equipped with a Ti:sapphire laser. The samples were excited at a wavelength of 552 nm with the signal for imaging within the range of 570−670 nm.

MTT Cell Viability Assay. MRC-5 cells (1×10^5) were treated with **GBYb001** for 24 h at six concentrations (1, 5, 15, 30, 50, and 100 μM). The cell monolayers were rinsed once with phosphate-buffered saline (PBS) and incubated with 500 mg mL^{-1} MTT solution. The cellular inhibitory potency of the mercury sensor was examined by treating the cells with MTT for 3 h to allow formazan production during cell metabolism. After that time, the formazan crystals were dissolved in DMSO with oscillation. Finally, the absorbance of the solution was measured with a Biotek PowerWave XS microplate reader at a wavelength of 570 nm.

Flow Cytometry Measurements of Cellular Uptake. MRC-5 cells (10^5 per sample) were seeded onto 35 mm Petri dishes and incubated overnight. Then the cells were incubated with 5 μM **GBYb001** for 0, 0.5, 1, or 2 h. Then, they were incubated with Hg^{2+} for a further 0.5 h. Cells were harvested with trypsin and washed twice with PBS. The uptake of **GBYb001** by MRC-5 cells was analyzed by a BD Accuri C6 flow cytometer. The cells were excited with a 488 nm argon laser, and the emission was collected in the FL-2 channel (with a 585 nm long-pass filter). A total of 10000 events were analyzed.

DFT Calculations. Geometry optimizations and TDDFT calculations were performed using ORCA 4.0.1[24] with BP86 and B3LYP functionals and the def2-TZVP or def2-SVP basis sets with the auxiliary basis set def2/J.[25,26] The optimized geometries did not have any imaginary frequencies.

Synthetic Procedures. *Synthesis of tert-Butyl (4-((2-(Hydroxymethyl)pyridin-4-yl)ethynyl)phenyl)carbamate (**8**).* To a solution of *tert*-butyl (4-iodophenyl)carbamate (2.88 g, 9.01 mmol) in 80 mL of THF were added DIPEA (13.08 mL, 75.10 mmol), $Pd(PPh_3)_4$ (173 mg, 0.15 mmol), CuI (57 mg, 0.30 mmol), and (4-ethynylpyridin-2-yl)methanol (**7**; 1.00 g, 7.51 mmol) under a nitrogen atmosphere. The reaction mixture was stirred at room temperature for 3 days. A 100 mL portion of water was added, and the contents were extracted with DCM (100 mL × 3). The organic phases were combined, dried over anhydrous Na_2SO_4, filtered, and purified by chromatography on silica gel with hexane/ethyl acetate (2/1 to 1/1, v/v) as eluent, affording the product as a white solid (2.10 g, 86.2% yield). ^1H NMR (400 MHz, $CDCl_3$): δ 8.53 (d, J = 5.1 Hz, 1H), 7.48 (d, J = 8.7 Hz, 2H), 7.39 (d, J = 8.7 Hz, 2H), 7.34 (s, 1H), 7.28 (d, J = 5.1 Hz, 1H), 6.61 (s, 1H), 4.76 (d, J = 4.1 Hz, 2H), 3.62 (t, J = 4.5 Hz, 1H), 1.53 (s, 9H). ^{13}C NMR (101 MHz, $CDCl_3$): δ 159.14, 152.31, 148.48, 139.43, 132.90, 132.40, 124.15, 122.18, 118.08, 116.14, 94.26, 86.08, 81.14, 64.05, 28.31. MALDI-TOF MS: calcd. for $[M + H^+]$ 325.1547, found 325.1552.

*Synthesis of tert-Butyl (4-((2-((4,7,10-Tris(2-(tert-butylamino)-2-oxoethyl)-1,4,7,10-tetraazacyclododecan-1-yl)methyl)pyridin-4-yl)-ethynyl)phenyl)carbamate (**9**).* To a solution of *tert*-butyl (4-((2-(hydroxymethyl)pyridin-4-yl)ethynyl)phenyl)carbamate (**8**; 973 mg, 3.00 mmol) and DIPEA (5.23 mL, 30.00 mmol) in 150 mL of dry DCM was added dropwise MsCl (0.70 mL, 9.00 mmol). The reaction mixture was stirred for 1 h at room temperature and then quenched with water (100 mL). Then it was extracted with DCM (100 mL × 3), washed with saturated aqueous $NaHCO_3$ (50 mL), and dried over anhydrous Na_2SO_4. The solvent was removed under reduced pressure, and the residue was quickly purified by chromatography on silica gel with DCM/ethyl acetate (1/1, v/v) as eluent, affording an intermediate as a white solid (1.11 g, 92.3% yield) which was immediately used for the next step. To a solution of the intermediate (1.05 g, 2.61 mmol) and K_2CO_3 (2.77 g, 20.07 mmol) in ACN (250 mL) was added 2,2′,2′′-(1,4,7,10-tetraazacyclododecane-1,4,7-triyl)-tris(*N*-(*tert*-butyl)acetamide) (**5**; 1.03 g, 2.01 mmol). The reaction mixture was stirred at 50 °C for 19 h. The solid was filtered off, and the solvent was removed. The residue was purified by chromatography on neutral Al_2O_3 with DCM/methanol (50/1, v/v) as eluent, affording the product as a yellow solid (1.60 g, 90.0% yield in two steps). ^1H NMR (400 MHz, DMSO): δ 9.68 (s, 1H), 8.36 (d, J = 5.1 Hz, 1H), 7.83 (s, 2H), 7.65 (s, 1H), 7.56 (s, 1H), 7.53 (d, J = 8.8 Hz, 2H), 7.46 (d, J = 8.8 Hz, 2H), 7.36 (d, J = 5.1 Hz, 1H), 3.97−3.44 (br, 2H),

DOI: 10.1021/acs.inorgchem.7b02243
Inorg. Chem. XXXX, XXX, XXX−XXX

3.19−2.56 (br, 12H), 2.46−1.82 (br, 10H), 1.48 (s, 9H), 1.29 (s, 9H), 1.21 (s, 18H). ^{13}C NMR (101 MHz, DMSO): δ 170.54, 169.90, 158.61, 152.55, 148.94, 140.89, 132.47, 131.21, 125.02, 123.39, 117.91, 114.21, 94.17, 85.88, 79.64, 58.04, 57.96, 57.26, 54.93, 50.42, 50.38, 28.28, 28.13, 28.08. MALDI-TOF MS: calcd for [M + Na$^+$] 840.5470, found 840.5500.

*Synthesis of 2,2′,2′′-(10-((4-((4-Aminophenyl)ethynyl)pyridin-2-yl)methyl)-1,4,7,10-tetraazacyclododecane-1,4,7-triyl)tris(N-(tert-butyl)acetamide) (**10**).* To a solution of *tert*-butyl (4-((2-((4,7,10-tris(2-(*tert*-butylamino)-2-oxoethyl)-1,4,7,10-tetraazacyclododecan-1-yl)methyl)pyridin-4-yl)ethynyl)phenyl)carbamate (**9**; 1.00 g, 1.22 mmol) in MeOH (30 mL) was added 6 M aqueous HCl (30 mL) under an ice bath. The reaction mixture was warmed to room temperature and stirred for 6 h. The pH of the solution was adjusted to 9 with 1.0 M aqueous NaOH, the solution was extracted with DCM (100 mL × 3), and the extracted material was dried over anhydrous Na_2SO_4. The solvent was removed, and the residue was purified by chromatography on neutral Al_2O_3 with elution by DCM/methanol (50/1, v/v), giving the product as a yellow solid (750 mg, 85.5% yield). ^{1}H NMR (400 MHz, DMSO): δ 8.31 (d, J = 5.1 Hz, 1H), 7.82 (s, 2H), 7.65 (s, 1H), 7.43 (s, 1H), 7.28 (dd, J = 5.1, 1.4 Hz, 1H), 7.21 (d, J = 8.6 Hz, 2H), 6.56 (d, J = 8.6 Hz, 2H), 5.75 (s, 2H), 3.65 (br, 2H), 2.72 (br, 12H), 2.19 (br, 10H), 1.30 (s, 9H), 1.21 (s, 18H). ^{13}C NMR (101 MHz, DMSO): δ 170.52, 169.93, 158.42, 150.40, 148.86, 133.15, 132.01, 124.53, 123.04, 113.58, 106.68, 96.54, 84.62, 58.03, 57.36, 54.93, 50.43, 50.39, 28.28, 28.13. MALDI-TOF MS: calcd for [M + H$^+$] 718.5127, found 718.5089.

*Synthesis of 2-Oxo-2-(4-((4-((2-((4,7,10-tris(2-(tert-butylamino)-2-oxoethyl)-1,4,7,10-tetraazacyclododecan-1-yl)methyl)pyridin-4-yl)ethynyl)phenyl)carbamoyl)phenyl)ethyl Pyrrolidine-1-carbodithioate (**11**).* To a solution of 4-(2-((pyrrolidine-1-carbonothioyl)-thio)acetyl)benzoic acid (**3**; 172 mg, 0.56 mmol) in 25 mL of dry MeCN were added DIPEA (0.24 mL, 1.39 mmol), EDCI (160 mg, 0.84 mmol), and HOBt (112 mg, 0.84 mmol). The reaction mixture was stirred for 0.5 h at room temperature, and 2,2′,2′′-(10-((4-((4-aminophenyl)ethynyl)pyridin-2-yl)methyl)-1,4,7,10-tetraazacyclododecane-1,4,7-triyl)tris(*N*-(*tert*-butyl)acetamide) (**10**; 200 mg, 0.28 mmol) was added. The reaction mixture was stirred for another 36 h at room temperature. Most of the solvent was removed under reduced pressure, 30 mL of water was added, extraction with DCM (30 mL × 3) was performed, and the extractant was dried over anhydrous Na_2SO_4. The solvent was removed, and the residue was purified by chromatography on neutral Al_2O_3 with DCM/methanol (50/1, v/v) as eluent, giving the product as a yellow solid (164 mg, 58.6% yield). ^{1}H NMR (400 MHz, DMSO): δ 10.70 (s, 1H), 8.39 (d, J = 5.0 Hz, 1H), 8.19 (d, J = 8.5 Hz, 2H), 8.09 (d, J = 8.5 Hz, 2H), 7.91 (d, J = 8.8 Hz, 2H), 7.82 (s, 2H), 7.63 (d, J = 8.3 Hz, 2H), 7.59 (d, J = 8.6 Hz, 2H), 7.41 (d, J = 6.2 Hz, 1H), 4.98 (s, 2H), 3.73 (m, 6H), 2.66 (m, 12H), 2.39−1.87 (m, 14H), 1.30 (s, 9H), 1.22 (s, 18H). ^{13}C NMR (101 MHz, DMSO): δ 192.84, 189.99, 170.55, 169.89, 165.12, 158.67, 148.97, 140.23, 138.59, 133.14, 132.39, 131.06, 128.24, 125.14, 123.47, 120.22, 116.17, 113.56, 93.83, 86.40, 58.10, 57.90, 57.22, 55.40, 54.93, 50.81, 50.41, 50.35, 49.39, 43.35, 28.27, 28.12, 25.74, 23.88. MALDI-TOF MS: calcd for [M + Na$^+$] 1031.5334, found 1031.5319.

*Synthesis of 2-Hydrazono-2-(4-((4-((2-((4,7,10-tris(2-(tert-butylamino)-2-oxoethyl)-1,4,7,10-tetraazacyclododecan-1-yl)methyl)-pyridin-4-yl)ethynyl)phenyl)carbamoyl)phenyl)ethyl Pyrrolidine-1-carbodithioate (**12**).* To a solution of 2-oxo-2-(4-((4-((2-((4,7,10-tris(2-(*tert*-butylamino)-2-oxoethyl)-1,4,7,10-tetraazacyclododecan-1-yl)methyl)pyridin-4-yl)ethynyl)phenyl)carbamoyl)phenyl)ethyl pyrrolidine-1-carbodithioate (**11**; 230 mg, 0.23 mmol) in THF (12 mL) and ethanol (12 mL) were added hydrazine hydrate (0.23 mL) and acetic acid (0.23 mL). Then the reaction mixture was heated to reflux and stirred for 2 h. The contents were cooled, and most of the solvent was removed. A 40 mL portion of water and 3 mL of saturated aqueous $NaHCO_3$ were added, followed by extraction with DCM (30 mL × 3) and drying over anhydrous Na_2SO_4. The solvent was removed, and the residue was chromatographed on neutral Al_2O_3 with DCM/methanol (50/1, v/v) as eluent, giving the product as a yellow solid (128 mg, 54.9% yield). ^{1}H NMR (400 MHz, DMSO): δ 10.46 (s, 1H), 8.38 (d, J = 5.1 Hz, 1H), 7.92 (m, 4H), 7.83 (s, 2H), 7.75 (d, J = 8.6 Hz, 2H), 7.65 (s, 1H), 7.61 (s, 1H), 7.56 (d, J = 8.7 Hz, 2H), 7.40 (dd, J = 5.1, 1.1 Hz, 1H), 7.32 (s, 2H), 4.61 (s, 2H), 3.71 (m, 6H), 2.66 (br, 12H), 2.40−1.80 (m, 14H), 1.30 (s, 9H), 1.22 (s, 18H). ^{13}C NMR (101 MHz, DMSO) δ 189.99, 170.54, 169.88, 165.43, 158.65, 148.96, 141.07, 140.54, 135.79, 132.66, 132.33, 131.10, 127.92, 125.10, 124.25, 123.45, 120.05, 115.76, 93.94, 86.27, 58.07, 57.87, 57.21, 55.56,50.59, 50.40, 50.34, 29.34, 28.26, 28.11, 25.57, 23.73. MALDI-TOF MS: calcd for [M + H$^+$] 1023.5783, found 1023.5765.

*Synthesis of 2-((3′,6′-Bis(diethylamino)-3-oxospiro[isoindoline-1,9′-xanthen]-2-yl)imino)-2-(4-((4-((2-((4,7,10-tris(2-(tert-butylamino)-2-oxoethyl)-1,4,7,10-tetraazacyclododecan-1-yl)methyl)-pyridin-4-yl)ethynyl)phenyl)carbamoyl)phenyl)ethyl Pyrrolidine-1-carbodithioate (**13**; **GB001**).* Rhodamine B (43 mg, 0.10 mmol) and $POCl_3$ (0.20 mL) were refluxed in 1,2-dichloroethane (4 mL) for 5 h, and then the solvent was removed. The obtained crude rhodamine B acid chloride was dissolved in 10 mL of dry DCM together with trimethylamine (0.30 mL) and 2-hydrazono-2-(4-((4-((2-((4,7,10-tris(2-(*tert*-butylamino)-2-oxoethyl)-1,4,7,10-tetraazacyclododecan-1-yl)methyl)pyridin-4-yl)ethynyl)phenyl)carbamoyl)phenyl)ethyl pyrrolidine-1-carbodithioate (**12**; 50 mg, 0.05 mmol) and stirred for 12 h at room temperature. After addition of 10 mL of water, extraction with DCM (10 mL × 4), and drying over anhydrous Na_2SO_4, the crude product was purified by chromatography on silica gel with DCM/MeOH (100/1 to 50/1, v/v) to give the desired product as a red solid (50 mg, 71.0% yield). ^{1}H NMR (400 MHz, DMSO): δ 10.51 (s, 1H), 8.38 (d, J = 5.1 Hz, 1H), 7.88 (m, 7H), 7.62 (m, 8H), 7.39 (d, J = 5.8 Hz, 1H), 7.20 (d, J = 6.8 Hz, 1H), 6.49 (d, J = 8.8 Hz, 2H), 6.43−6.27 (m, 4H), 4.73 (s, 2H), 3.74 (m, 4H), 3.31 (q, 8H), 2.71 (br, 14H), 2.33 (br, 8H), 2.00−1.77 (br, 6H), 1.30 (s, 9H), 1.21 (s, 18H), 1.08 (t, J = 6.9 Hz, 12H). ^{13}C NMR (101 MHz, DMSO): δ 189.43, 170.56, 169.90, 165.51, 165.01, 160.36, 158.68, 153.15, 150.81, 148.97, 148.35, 140.26, 138.02, 136.26, 133.37, 132.38, 131.07, 129.77, 128.93, 128.27, 127.86, 127.17, 125.14, 124.06, 123.47, 123.19, 120.08, 116.04, 107.93, 105.97, 97.24, 93.84, 86.36, 66.97, 58.10, 57.88, 57.24, 55.78, 54.92, 50.41, 50.36, 30.71, 28.26, 28.12, 25.50, 23.65, 12.41. MALDI-TOF MS: calcd for [M + Na$^+$] 1469.7753, found 1469.7783

*Synthesis of GBYb001 (**14a**).* To a solution of **13** (**GB001**; 14 mg. 0.01 mmol) in 1.0 mL of MeOH was added 0.01 M aqueous $YbCl_3$ (1.05 mL, 0.0105 mmol), and the mixture was stirred for 24 h at room temperature. The solvent was removed, and the residue was dissolved in 2 mL of water and washed with DCM (2 mL × 3). The water was removed, and the residue was dried under vacuum, giving a purple solid as product (15 mg, 83.3% yield). ESI-MS: calcd for [M − H_2O − 3Cl$^-$ − 2H$^+$] 1618.7, found 1618.9; calcd for [M − H_2O − 3Cl$^-$ − H$^+$]/2 809.9. HPLC retention time: 16.07 min.

*Synthesis of GBLa001 (**14b**).* To a solution of **13** (**GB001**; 5 mg, 0.0035 mmol) in 0.7 mL of MeOH was added 0.005 M aqueous $LaCl_3$ (0.71 mL, 0.00354 mmol), and the mixture was stirred for 24 h at room temperature. The solvent was removed, and the residue was dissolved in 2 mL of water and washed with DCM (3 × 1 mL). The water was removed, and the residue was dried under vacuum, giving a purple solid as the product (5.8 mg, 93.3% yield). ^{1}H NMR (400 MHz, DMSO): δ 10.51 (s, 1H), 8.38 (d, J = 5.2 Hz, 1H), 7.95−7.76 (m, 7H), 7.74−7.52 (m, 8H), 7.39 (d, J = 5.2 Hz, 1H), 7.20 (d, J = 7.2 Hz, 1H), 6.49 (d, J = 8.9 Hz, 2H), 6.42−6.27 (m, 4H), 4.72 (s, 4H), 3.74 (s, 8H), 3.31−3.29 (m, 14H), 2.65 (d, J = 14.3 Hz, 8H), 2.28 (d, J = 35.9 Hz, 6H), 1.89 (dd, J = 21.8, 6.3 Hz, 9H), 1.30 (s, 1H), 1.18 (d, J = 26.4 Hz, 18H), 1.08 (7, J = 6.9 Hz, 12H). HPLC retention time: 16.06 min.

*Synthesis of GBYb002 (**15**).* To a solution of **11** (**GB002**; 6.5 mg. 0.0065 mmol) in 1 mL of MeOH was added 0.005 M aqueous $YbCl_3$ (1.00 mL, 0.0065 mmol), and the mixture was stirred for 24 h at room temperature. The solvent was removed, and the residue was dissolved in 2 mL of water and washed with DCM (3 × 1 mL). The water was removed, and the residue was dried under vacuum, giving a yellow solid as the product (8.0 mg, 92.0% yield). HPLC retention time: 15.02 min.

DOI: 10.1021/acs.inorgchem.7b02243
Inorg. Chem. XXXX, XXX, XXX−XXX

■ ASSOCIATED CONTENT

Supporting Information

The Supporting Information is available free of charge on the ACS Publications website at DOI: 10.1021/acs.inorgchem.7b02243.

Details of the experimental procedure, synthesis, characterization data, photophysical properties, mechanism, cytotoxicity, and cellular uptake (PDF)

■ AUTHOR INFORMATION

Corresponding Authors

*E-mail for D.J.: dayong.jin@uts.edu.au.
*E-mail for P.A.T.: peter.a.tanner@gmail.com.
*E-mail for K.-L.W.: klwong@hkbu.edu.hk.

ORCID

Hongguang Li: 0000-0002-6579-7300
Dayong Jin: 0000-0003-1046-2666
Peter A. Tanner: 0000-0002-4681-6203
Ka-Leung Wong: 0000-0002-3750-5980

Notes

The authors declare no competing financial interest.

■ ACKNOWLEDGMENTS

This work was funded by grants from The Hong Kong Research Grants Council (HKBU 22301615) and Hong Kong Baptist University (FRG 1/16-17/016 and SDF 15-0324-P03).

■ REFERENCES

(1) Sun, Q.; Aguila, B.; Perman, J.; Earl, L. D.; Abney, C. W.; Cheng, Y.; Wei, H.; Nguyen, N.; Wojtas, L.; Ma, S. Postsynthetically modified covalent organic frameworks for efficient and effective mercury removal. *J. Am. Chem. Soc.* **2017**, *139*, 2786−2793.

(2) Yan, Z.; Xue, H.; Berning, K.; Lam, Y. W.; Lee, C. S. Identification of multifunctional graphene-gold nanocomposite for environment-friendly enriching, separating, and detecting Hg^{2+} simultaneously. *ACS Appl. Mater. Interfaces* **2014**, *6*, 22761−22768.

(3) Li, Y.; He, S.; Lu, Y.; Zeng, X. Novel hemicyanine dye as colorimetric and fluorometric dual-modal chemosensor for mercury in water. *Org. Biomol. Chem.* **2011**, *9*, 2606−2609.

(4) Ko, S.-K.; Yang, Y.-K.; Tae, J.; Shin, I. In vivo monitoring of mercury ions using a rhodamine-based molecular probe. *J. Am. Chem. Soc.* **2006**, *128*, 14150−14155.

(5) Huang, N.; Zhai, L.; Xu, H.; Jiang, D. Stable covalent organic frameworks for exceptional mercury removal from aqueous solutions. *J. Am. Chem. Soc.* **2017**, *139*, 2428−2434.

(6) Duan, W.; Han, Y.; Liu, Q.; Cui, J.; Gong, S.; Ma, Y.; Zhang, C.; Sun, Z. Design and synthesis of novel rhodamine-based chemodosimeters derived from [2.2]paracyclophane and their application in detection of Hg^{2+} ion. *Tetrahedron Lett.* **2017**, *58*, 271−278.

(7) Liu, B. Highly sensitive oligonucleotide-based fluorometric detection of mercury(II) in aqueous media. *Biosens. Bioelectron.* **2008**, *24*, 756−760.

(8) Taki, M.; Akaoka, K.; Iyoshi, S.; Yamamoto, Y. Rosamine-based fluorescent sensor with femtomolar affinity for the reversible detection of a mercury ion. *Inorg. Chem.* **2012**, *51*, 13075−71307.

(9) Zhang, T.; Chan, C. F.; Lan, R.; Wong, W. K.; Wong, K. L. Highly selective and responsive visible to NIR ytterbium emissive probe for monitoring mercury(II). *Chem. - Eur. J.* **2014**, *20*, 970−973.

(10) Kim, S. K.; Swamy, K. M. K.; Chung, S.-Y.; Kim, H. N.; Kim, M. J.; Jeong, Y.; Yoon, J. New fluorescent and colorimetric chemosensors based on the rhodamine and boronic acid groups for the detection of Hg^{2+}. *Tetrahedron Lett.* **2010**, *51*, 3286−3289.

(11) Yang, Y.-K.; Yook, K.-J.; Tae, J. A rhodamine-based fluorescent and colorimetric chemodosimeter for the rapid detection of Hg^{2+} ions in aqueous media. *J. Am. Chem. Soc.* **2005**, *127*, 16760−16761.

(12) Ahamed, B. N.; Ghosh, P. An integrated system of pyrene and rhodamine-6G for selective colorimetric and fluorometric sensing of mercury(II). *Inorg. Chim. Acta* **2011**, *372*, 100−107.

(13) Broussard, J. A.; Rappaz, B.; Webb, D. J.; Brown, C. M. Fluorescence resonance energy transfer microscopy as demonstrated by measuring the activation of the serine/threonine kinase Akt. *Nat. Protoc.* **2013**, *8*, 265−281.

(14) Ning, Y.; Ke, X. S.; Hu, J. Y.; Liu, Y. W.; Ma, F.; Sun, H. L.; Zhang, J. L. Bioinspired orientation of beta-substituents on porphyrin antenna ligands switches ytterbium(III) NIR emission with Thermosensitivity. *Inorg. Chem.* **2017**, *56*, 1897−1905.

(15) Ke, X. S.; Yang, B. Y.; Cheng, X.; Chan, S. L.; Zhang, J. L. Ytterbium(III) porpholactones: beta-lactonization of porphyrin ligands enhances sensitization efficiency of lanthanide near-infrared luminescence. *Chem. - Eur. J.* **2014**, *20*, 4324−4333.

(16) Heffern, M. C.; Matosziuk, L. M.; Meade, T. J. Lanthanide probes for bioresponsive imaging. *Chem. Rev.* **2014**, *114*, 4496−539.

(17) Hildebrandt, N.; Spillmann, C. M.; Algar, W. R.; Pons, T.; Stewart, M. H.; Oh, E.; Susumu, K.; Diaz, S. A.; Delehanty, J. B.; Medintz, I. L. Energy transfer with semiconductor quantum dot bioconjugates: a versatile platform for biosensing, energy harvesting, and other developing applications. *Chem. Rev.* **2017**, *117*, 536−711.

(18) Hu, J.-Y.; Ning, Y.; Meng, Y.-S.; Zhang, J.; Wu, Z.-Y.; Gao, S.; Zhang, J.-L. Highly near-IR emissive ytterbium(III) complexes with unprecedented quantum yields. *Chem. Sci.* **2017**, *8*, 2702−2709.

(19) Li, H.; Lan, R.; Chan, C.-F.; Bao, G.; Xie, C.; Chu, P.-H.; Tai, W. C. S.; Zha, S.; Zhang, J.-X.; Wong, K.-L. A luminescent lanthanide approach towards direct visualization of primary cilia in living cells. *Chem. Commun.* **2017**, *53*, 7084−7087.

(20) Li, H.; Lan, R.; Chan, C.-F.; Jiang, L.; Dai, L.; Kwong, D. W. J.; Lam, M. H.-W.; Wong, K.-L. Real-time in situ monitoring via europium emission of the photo-release of antitumor cisplatin from a Eu-Pt complex. *Chem. Commun.* **2015**, *51*, 14022−14025.

(21) Sitong, C.; Weiming, G.; Bo, Z.; Tonglai, Z.; Li, Y. Methyl carbazate energetic complexes: Transition metal perchlorates − Syntheses, crystal structures and properties. *Polyhedron* **2016**, *117*, 110−116.

(22) Bourson, J.; Pouget, J.; Valeur, B. Ion-responsive fluorescent compounds. 4. effect of cation binding on the photophysical properties of a coumarin linked to monoaza- and diaza-crown ethers. *J. Phys. Chem.* **1993**, *97*, 4552−4557.

(23) Smith, A. M.; Mancini, M. C.; Nie, S. Bioimaging: second window for in vivo imaging. *Nat. Nanotechnol.* **2009**, *4*, 710−711.

(24) Neese, F. The ORCA program system. *WIREs Comput. Mol. Sci.* **2012**, *2*, 73−78.

(25) Weigend, F. Accurate Coulomb-fitting basis sets for H to Rn. *Phys. Chem. Chem. Phys.* **2006**, *8*, 1057−1065.

(26) Weigend, F.; Ahlrichs, R. Balanced basis sets of split valence, triple zeta valence and quadruple zeta valence quality for H to Rn: Design and assessment of accuracy. *Phys. Chem. Chem. Phys.* **2005**, *7*, 3297−3305.

(27) Zhang, T.; Zhu, X.; Cheng, C. C. W.; Kwok, W.-M.; Tam, H.-L.; Hao, J.; Kwong, D. W. J.; Wong, W.-K.; Wong, K.-L. Water-soluble mitochondria-specific ytterbium complex with impressive NIR emission. *J. Am. Chem. Soc.* **2011**, *133*, 20120−20122.

DOI: 10.1021/acs.inorgchem.7b02243
Inorg. Chem. XXXX, XXX, XXX−XXX